ACS APPLIED MATERIALS & INTERFACES
Letter
www.acsami.org

Green Facile Scalable Synthesis of Titania/Carbon Nanocomposites: New Use of Old Dental Resins

Ying Xiao,[†,‡] Xiaoyan Wang,[†,‡,§] Yonggao Xia,[‡] Yuan Yao,[⊥] Ezzeldin Metwalli,[⊥] Qian Zhang,[‡] Rui Liu,[#] Bao Qiu,[‡] Majid Rasool,[⊥] Zhaoping Liu,[‡] Jian-Qiang Meng,[§] Ling-Dong Sun,[#] Chun-Hua Yan,[#] Peter Müller-Buschbaum,[⊥] and Ya-Jun Cheng*,[‡]

[‡]Ningbo Institute of Materials Technology and Engineering, Chinese Academy of Sciences, 1219 Zhongguan West Road, Zhenhai District, Ningbo, Zhejiang Province 315201, P. R. China

[§]Tianjin Polytechnic University, State Key Laboratory of Hollow Fiber Membrane Materials & Processes, Tianjin 300387, P. R. China

[⊥]Physik-Department, Lehrstuhl für Funktionelle Materialien, Technische Universität München, James-Franck-Strasse 1, 85748 Garching, Germany

[#]Beijing National Laboratory for Molecular Sciences, State Key Laboratory of Rare Earth Materials Chemistry and Applications & PKU-HKU Joint Lab on Rare Earth Materials and Bioinorganic Chemistry, College of Chemistry and Molecular Engineering, Peking University, Beijing 100871, P. R. China

Supporting Information

ABSTRACT: A green facile scalable method inspired by polymeric dental restorative composite is developed to synthesize TiO_2/carbon nanocomposites for manipulation of the intercalation potential of TiO_2 as lithium-ion battery anode. Poorly crystallized TiO_2 nanoparticles with average sizes of 4−6 nm are homogeneously embedded in carbon matrix with the TiO_2 mass content varied between 28 and 65%. Characteristic discharge/charge plateaus of TiO_2 are significantly diminished and voltage continues to change along with proceeding discharge/charge process. The tap density, gravimetric and volumetric capacities, and cyclic and rate performance of the TiO_2/C composites are effectively improved.

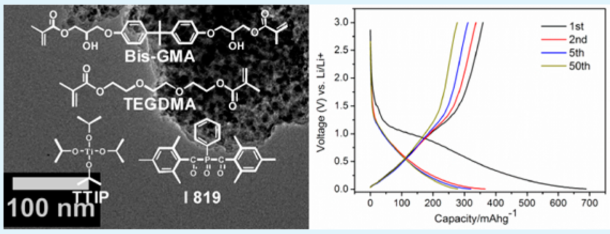

KEYWORDS: *titania/carbon nanocomposites, nanoparticles, photo polymerization, dental methacrylate resin, lithium-ion battery anode*

Titanium dioxide (TiO_2) is a promising lithium ion battery (LIB) anode because of low cost, good cyclic stability, high theoretical capacity, and environmental friendliness.[1−3] Compared to commercialized graphite anode, the high intercalation potential of TiO_2 (1.7 V vs 0.1 V) provides good operation safety during repeated charge/discharge process.[1] Nevertheless, the high intercalation potential also lowers the open circuit voltage and inevitably reduces the total energy output of the full LIBs. It is essential to lower down the intercalation potential appropriately, while not sacrificing the capacity, rate and cyclic performance of TiO_2. However, studies on the intercalation potential manipulation of TiO_2 have been rarely addressed. It is reported that amorphous TiO_2 exhibits different discharge/charge behavior as compared with crystalline TiO_2.[4−9] The discharge/charge plateaus are significantly weakened with respect to typical discharge/charge behavior of TiO_2. Continuous voltage drop/increase is observed with proceeding discharge/charge process.[4−9]

Besides the intercalation potential manipulation, the control over morphology,[10−12] surface carbon coating,[13] and tap density of TiO_2 is also very important.[14] Immense research work has been devoted to synthesizing nanostructured TiO_2 with surface carbon coating.[3,15−18] Synthetic methods frequently exploited include hard/soft template, emulsification, hydro/solvothermal, and template free synthesis.[10−12,19−21]Organic molecules such as homopolymers,[15,20,22] amphiphilic block copolymers,[21,23] small molecule surfactants,[20,24] and phenolic resins,[20,23] have been used as templating agents and/or carbon source to synthesize TiO_2 nanostructures. Despite the great success of these strategies, challenges still remain:(1) huge amounts of water and/or organic solvents are used; (2) many synthetic methods are time-consuming and difficult to scale up; (3) the tap densities of the nanostructured powders are normally quite low, leading to inferior volumetric capacities, which limit its applications in portable and wearable electronic devices.[14]

In the present work, we report a new strategy to synthesize TiO_2/carbon nanocomposites inspired by polymeric dental restorative composite, which has achieved a great clinical success since the 1960s.[25] With this strategy, morphology

Received: September 10, 2014
Accepted: October 22, 2014
Published: October 22, 2014

Scheme 1. Synthesis of TiO_2 and TiO_2/C Nanocomposites Based on Dental Methacrylate Monomers

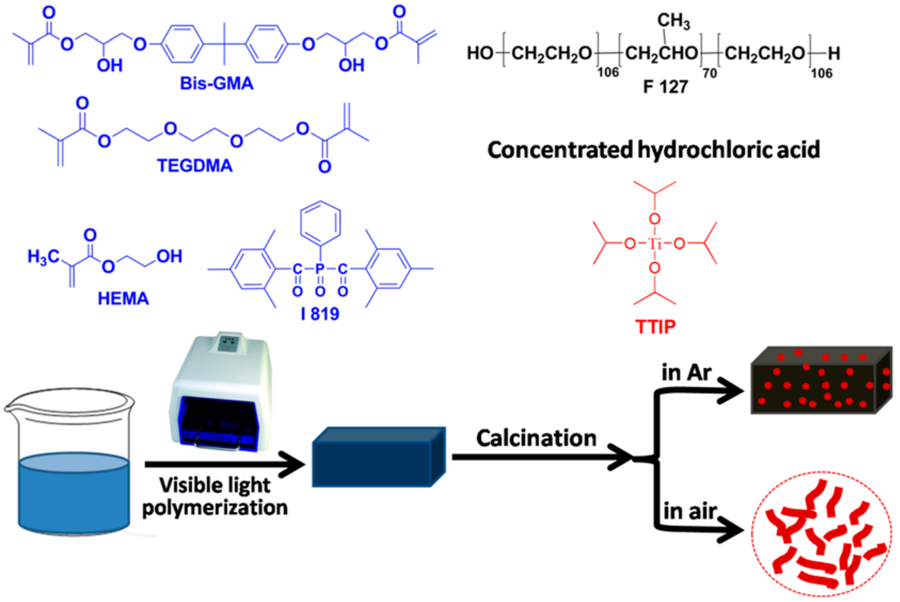

control, surface carbon coating, and intercalation potential manipulation of TiO_2 can be achieved simultaneously (Scheme 1).

Typical dental resin monomers of bisphenol A-glycidyl methacrylate (Bis-GMA, B), triethylene glycol dimethacrylate (TEGDMA, T), and 2-hydroxyethyl methacrylate (HEMA) are used as reaction medium to replace conventional solvents (1.6 g of B, 2.4 g of T, and 2 g of HEMA). An energy saving visible light polymerization process initiated by Bis (2, 4, 6-trimethylbenzoyl)-phenyl phosphine oxide (IRGACURE 819, I-819, 2% by mass with respect to the total mass of the resins) is applied, which can be completed within the time range from seconds to minutes.[26] Titanium tetraisopropoxide (TTIP, 0−8 g) is used as the precursor of TiO_2, which can be incorporated into the resin matrix via coordination bonds. Concentrated hydrochloric acid (0.5 g) is added to control the sol−gel reaction of TTIP. Pluronic type of amphiphilic block copolymer of poly(ethylene oxide)-*block*-poly(propylene oxide)-*block*-poly(ethylene oxide) (F127, 0.5 g) is added to adjust the morphology of TiO_2.[23] Via photo polymerization, solid composites composed of cross-linked methacrylate network and titania related species are formed, which can be converted to TiO_2/C nanocomposites through calcination in argon atmosphere. TiO_2 nanoparticles are homogeneously embedded in the *in situ* formed carbon matrix from the decomposition of the cross-linked methacrylate. Scanning electron microscopy (SEM), transmission electron microscopy (TEM), X-ray photoelectron microscopy (XPS), energy-dispersive X-ray spectroscopy (EDX), small-angle X-ray scattering (SAXS), X-ray diffraction (XRD), Raman, and thermogravimetric analysis (TGA) were used to characterize the samples. Thereafter, 2032-type coin cells composed of a cylindrical pad with 20 mm in diameter and 3.2 mm in height were fabricated using Lithium foil as the counter electrode to investigate the electrochemical performance of the composite anodes (see Figure S1 in the Supporting Information). Experimental details can be accessed in the Supporting Information.

This strategy has several distinct advantages. First, the use of methacrylate monomer as solvents completely circumvents the tedious, costly, and environment unfriendly solvent disposal process. Second, compared to other synthetic methods, the photo polymerization process is a fast green and energy saving process because it can be completed rather fast and no additional heating is required. Third, the dissolve of TTIP in the resin solution and instant formation of cross-linked methacrylate network by photo polymerization allow homogeneous fixation of the titania related species to the cross-linked polymer matrix. Morphology control of TiO_2 and surface modification by the in situ formed carbon during calcination can be achieved. Fourthly, the cross-linked methacrylate network with phenyl functional groups within Bis-GMA helps to improve the carbon yield during calcination. It is true that the synthesis of the dental resin monomers requires solvent; and calcination at high temperature demands energy. However, the process developed in this work is still regarded as a relatively green process in the sense of circumventing solvent disposal and application of visible-light-initiated photo polymerization.

The morphologies of the TiO_2/C nanocomposites after calcination in argon followed by ball milling are revealed by transmission electron microscopy (TEM) as shown in Figure 1. When the mass ratio of TTIP against the total mass of the solution constituents (M_{TTIP}) is 0.14, TiO_2 nanoparticles with an average size of around 4 nm are homogeneously embedded within the carbon matrix (Figure 1a). High-resolution transmission electron microscopy (HRTEM) and selected area electron diffraction (SAED) measurements indicate a poor crystallization of TiO_2 (Figure 1b). With increasing M_{TTIP}, the average sizes of the TiO_2 nanoparticles are increased to around 6 nm (Figure 1c, 1e, and 1g). Both HRTEM and SAED results indicate that the TiO_2 nanoparticles are partially crystallized into anatase phase (Figure 1d, f and h). Featureless structures with a broad size distribution are observed by scanning electron microscopy (SEM) with M_{TTIP} varied from 0.14 to 1.14 (see Figure S2 in the Supporting Information). Particles are randomly assembled together, where smaller particles reside on the surface of larger particles. The TiO_2 nanoparticles of 4−6 nm are hardly seen by SEM. It is due to the limited capability of SEM to detect such small particles on the surface

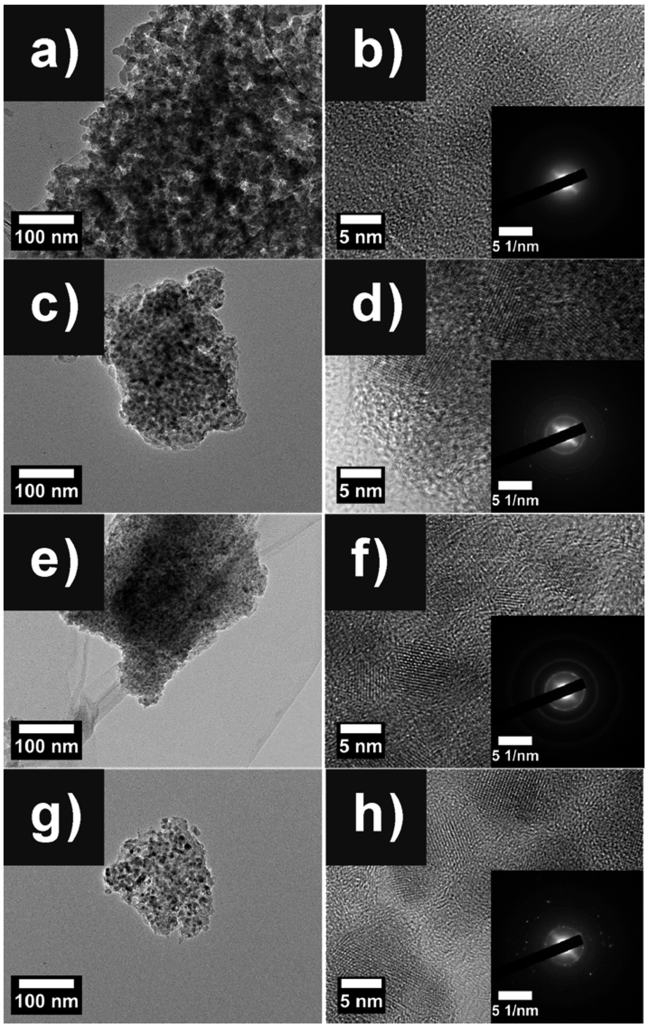

Figure 1. (a, c, e, g) TEM and (b, d, f, h) HRTEM images of the TiO_2/C nanocomposites prepared with different M_{TTIP}: (a, b) 0.14, (c, d) 0.29, (e, f) 0.57, and (g, h) 1.14. Insets: SAED patterns of each sample.

of bulk powders with irregular shape, rough surface, and broad size distribution. However, X-ray photoelectron spectroscopy (XPS) indicates the existence of TiO_2 within the composites (see Figure S3 in the Supporting Information), where Ti 2p3/2 and Ti 2p1/2 are located at 459.0 and 464.8 eV and O 1s is located at 530.0 eV, respectively. Furthermore, energy-dispersive X-ray spectroscopy (EDX) elemental mapping images prove the homogeneous distribution of titania species within the TiO_2/C composite over μm scale area (see Figure S4 in the Supporting Information). Small-angle X-ray scattering (SAXS) is used to investigate the average structures of the TiO_2/C composites (see Figure S5 in the Supporting Information). On the basis of the fitting models, bimodal pore size distribution exists with average sizes of 0.5 and 2 nm (see Figure S5b−d in the Supporting Information).[27,28] It is necessary to point out that the pores detected by X-ray likely refer to the carbon domains located around the TiO_2 nanoparticles. SAXS measures the contrast between titania and carbon since titania is embedded in the carbon matrix.

Unlike the TiO_2 nanoparticles of 4−6 nm formed via calcination in argon, wormlike TiO_2 nanoparticles are observed after calcination in air (see Figure S5 in the Supporting Information). With the M_{TTIP} of 0.14, the average length and width of the worm-like nanoparticles are 100 and 30 nm respectively (see Figure S5a in the Supporting Information), which are assembled into μm sized monolith (inset of Figure S5a in the Supporting Information). The fairly smooth surface indicates the uniform morphology of the worm-like particles organized with a good order. With the M_{TTIP} increased to 0.29, besides worm-like nanoparticles, spherical particles with the average size of around 50 nm are also present (see Figure S5b in the Supporting Information). With the M_{TTIP} of 0.57 and 1.14, irregularly shaped TiO_2 nanogranules are formed, which are randomly assembled (see Figure S5c, d in the Supporting Information). As a result, monoliths with quite rough surface are observed (insets of Figure S5c, d in the Supporting Information). The results suggest that with increasing amount of TTIP, a morphology transition from worm-like nanoparticles to irregular nanogranules is promoted by thermal driving force during calcination in air.

The distinct morphology difference of TiO_2 through calcination in different atmosphere is due to the in situ formed carbon from the decomposition of the cross-linked methacrylate network. The precursor of titania is homogeneously fixed to the cross-linked methacrylate network by forming coordination bonds between Ti and oxygen atoms within the resin matrix. Upon calcination in argon, the local titania related moieties are converted to tiny TiO_2 nanoparticles. However, further thermally induced growth and aggregation of neighboring TiO_2 nanoparticles are severely inhibited by the in situ formed carbon. As a result, only TiO_2 nanoparticles with very small size are formed within the carbon matrix. It is found that the average particle size is only increased slightly from 4 to 6 nm with the M_{TTIP} increased from 0.14 to 1.14. These results suggest that with increasing amount of TTIP, the in situ formed carbon can still effectively prevent the growth of the TiO_2 nanoparticles via an aggregation route.

The X-ray diffraction (XRD) results in Figure 2 shows that the TiO_2 calcined in air with the M_{TTIP} of 0.14, 0.29, and 0.57 are well-indexed to the anatase phase, whereas with the M_{TTIP} of 1.14, rutile becomes a dominant phase, coexisting with anatase. The sharp diffraction peaks imply that TiO_2 are crystallized quite well, where the crystallite sizes are in the range of 27−41 nm according to the Debye−Scherer equation. However, with the M_{TTIP} of 1.14, rutile forms as a major content and anatase becomes a minor phase.

It is reported that the anatase-to-rutile transformation can be influenced by various parameters such as particle morphology, purity, precursor, atmosphere, and reaction conditions.[29] In this work, the coordination pattern, local environment, and nanocrystals packing of the titania related clusters may be modified with excessive amount of TTIP present in resin. As a result, rutile instead of anatase is formed as a major content after calcination in air. Figure 2b shows that the TiO_2 nanoparticles embedded in the carbon matrix are mainly of anatase phase with tiny amount of rutile phase observed with the M_{TTIP} of 0.29 and 1.14. Compared to the TiO_2 calcined in air, the peaks are much broader. It indicates that the crystallization of TiO_2 within the carbon matrix is rather limited. Correspondingly, the average crystallite sizes are only around 7 nm according to Debye-Scherer equation.

The thermogravimetric analysis (TGA) results show that the TiO_2/C nanocomposites prepared with the M_{TTIP} of 0.14 has a carbon content of 72% by mass (Figure 2c). The cross-linking network of the methacrylate polymer and the phenyl ring structure within Bis-GMA are supposed to make significant

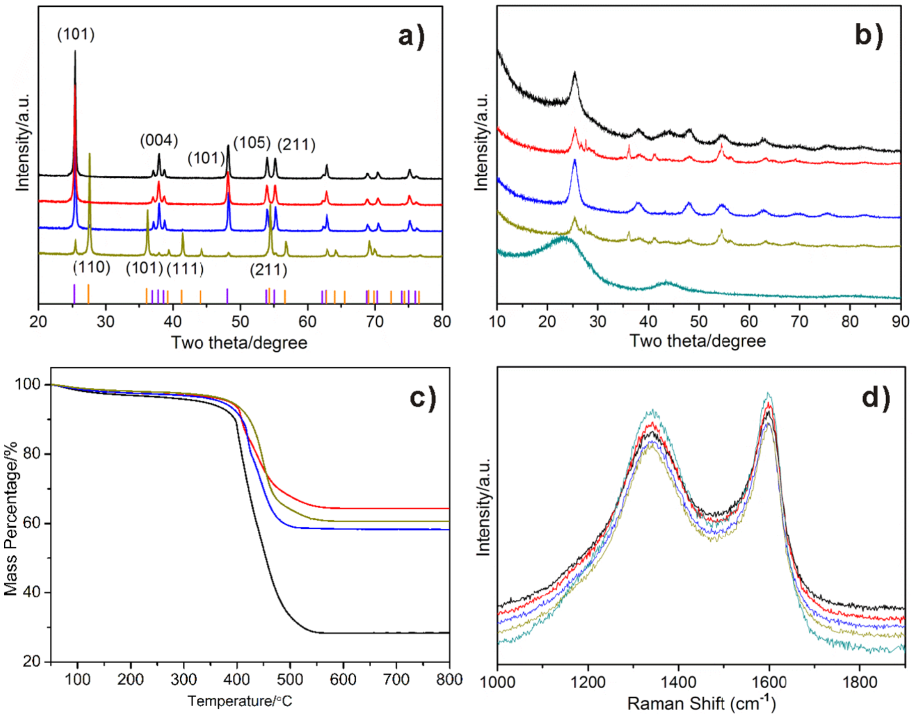

Figure 2. XRD patterns of the (a) TiO_2 and (b) TiO_2/C composites, (c) TGA and (d) Raman patterns of the TiO_2/C composites prepared with different M_{TTIP}. Black, 0.14; red, 0.29; blue, 0.57; yellow, 1.14; and green (in panels b and d), 0. Lines in panel a are standard XRD patterns of crystalline TiO_2: purple, anatase; orange, rutile.

contribution to the formation of carbon. With the M_{TTIP} doubled to 0.29, the carbon content is decreased to around 35%. However, as the M_{TTIP} further increases to 0.57, and 1.14, the carbon contents do not change significantly, which are still around 40 and 38%, respectively. Considering that the TTIP amount is significantly increased, the overall improved carbon yield is because of the enhanced cross-linking of the methacrylate polymer network brought by the Titanium ions. The broad peaks in the XRD profile of bare carbon indicate the formation of graphite type carbon after calcination in argon.

Raman spectra of the TiO_2/C composites indicate that both graphite type carbon (1600 cm^{-1}, G band) and disordered carbon (1350 cm^{-1}, D band) coexist within the carbon matrix (Figure 2d). The shape of the D band and G band, and the integral intensity ratios between the D band and G band do not change significantly with the M_{TTIP} changed from 0 to 1.14 (area ratio of D band/G band: 1.6). It implies that the incorporation of TTIP into the methacrylate network does not significantly modify the nature of the carbon.

The discharge/charge curves of TiO_2 powders at the current density of 0.2 *C* (1 *C* = 335 mAh/g) are shown in Figure 3a and Figure S7 in the Supporting Information. Typical plateaus of anatase TiO_2 are observed in the discharge/charge curves with the M_{TTIP} varied from 0.14 to 0.57. But with the M_{TTIP} of 1.14, the plateau is significantly lowered because rutile instead of anatase becomes the dominate phase. It seems that the first discharge/charge capacities are significantly influenced by the morphology of TiO_2. With the M_{TTIP} of 0.14 and 0.29, very similar discharge/charge capacities are observed, where the morphologies of the wormlike nanoparticles resemble each other. With the M_{TTIP} of 0.57, inferior discharge/charge capacities are observed, where irregularly organized nanogranules are formed. The patterns of the discharge/charge of each sample curves are quite similar to increasing cycles. But the capacities decrease gradually and the plateaus are correspondingly narrowed. After 50 cycles at 0.2 *C*, around 50% of the charge capacities are lost. The results indicate that the bare TiO_2 nanoparticles do not have good cyclic stability.

Compared to bare TiO_2, the TiO_2/C nanocomposites exhibit distinctly different discharge/charge behaviors (Figure 3b–f). Typical discharge/charge curve of bare carbon anode is shown in Figure 3b. No obvious plateaus are observed. The first discharge/charge capacities reach 491 mAh/g and 255 mAh/g respectively with a first coulomb efficiency of 52%. The patterns of the second, fifth, and 50th discharge/charge curves do not change significantly with the capacities gradually increased to 345 mAh/g. Concerning the TiO_2/C nanocomposites, the patterns of the discharge/charge curves (Figure 3c–f) resemble the curve of the bare carbon. With the M_{TTIP} of 0.14 (TiO_2/carbon mass ratio: 28/72), typical plateau of TiO_2 is not visible. The first discharge/charge curves reach 689 mAh/g and 359 mAh/g respectively, with the first coulomb efficiency of 52%. After 50 cycles, both the discharge and charge capacities reach around 277 mAh/g. When the M_{TTIP} is increased to 0.29 (TiO_2/carbon mass ratio: 65/35), very small plateaus at around 1.7 and 2.0 V appear in the discharge and charge curves respectively (Figure 3d). The plateaus imply the lithiation/delithiation processes of anatase TiO_2. The first discharge/charge curves reach 583 mAh/g and 266 mAh/g respectively, with the first coulomb efficiency of 46%. After 50 cycles, the discharge/charge capacities reach around 229 mAh/g. With the M_{TTIP} increased to 0.57 (TiO_2/carbon mass ratio: 58/42), small plateaus at 1.7 and 2.0 V still exist (Figure 3e). The first discharge/charge curves reach 556 mAh/g and 251 mAh/g respectively, with the first coulomb efficiency of 45%. After 50 cycles, the discharge/charge capacities are ca. 218 mAh/g. With the M_{TTIP} of 1.14 (TiO_2/C mass ratio: 60:40), only tiny turning points at around 1.7 V are observed in the discharge curve

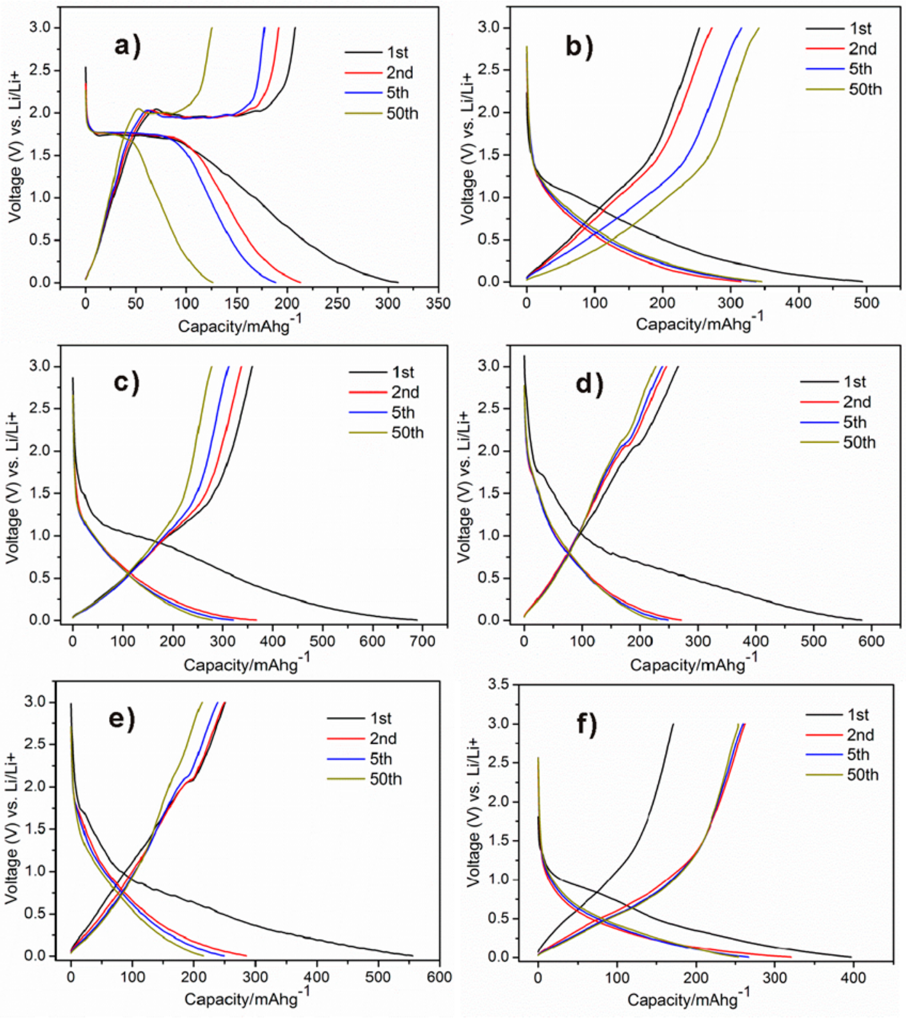

Figure 3. Charge/discharge curves of(a) the bare TiO_2 ands (b–f) TiO_2/C composite prepared with different M_{TTIP}: (a) 0.29, (b) 0, (c) 0.14, (d) 0.29, (e) 0.57, and (f) 1.14.

(Figure 3f). Even though the capacities of the first discharge process are less compared to other TiO_2/C composites (only 170 mAh/g for charge capacity), the capacities are improved with further cycles and reach 254 mAh/g after 50 cycles.

The dramatic modification of the discharge/charge behavior of the TiO_2/C nanocomposites is supposed to be the synergistic effects of the poor crystallization of TiO_2 and homogeneous distribution of the TiO_2 nanoparticles within the carbon matrix. It is reported that the appearance of the characteristic plateau originates from the lithiation/delithiation process of crystalline TiO_2, where Li_xTiO_2 is formed upon lithiation.[30] However, when TiO_2 of poor crystallization is exploited as anode, no distinct stable lithiation/delithiation phase is formed. As a result, the plateaus are diminished and voltage continues to change along with proceeding lithiation/delithiation process. Furthermore, because TiO_2 nanoparticles with the size of 4–6 nm are homogeneously embedded within the carbon matrix, the patterns of the discharge/charge curves resemble the standard pattern of the bare carbon anode. Even though the mass ratio of TiO_2 is increased to more than 65%, the patterns still do not change significantly, where only very narrow plateaus are observed. This finding is confirmed by cyclic voltammetry results (see Figure S8 in the Supporting Information). The well-crystallized TiO_2 powder exhibits distinct characteristic anodic/cathodic peaks (see Figure S8a in the Supporting Information). Concerning bare carbon, a broad peak at 0.9 V and a weak peak at 1.6 V appear in the first cycle, due to the formation of solid electrolyte interface (SEI) and irreversible lithium insertion into the pores of carbon (see Figure S8b in the Supporting Information). From the second cycle, no obvious peaks are observed. Regarding the TiO_2/C nanocomposites, the patterns of the CV curves are very similar to that of the bare carbon, except the existence of weak peaks from the second cycle due to TiO_2 (see Figure S8c–f in the Supporting Information).

The tap densities and volumetric capacities of the composites are also investigated (see Figure S9 in the Supporting Information). It is found that the incorporation of TiO_2 nanoparticles into the carbon matrix significantly improves the tap density, which is increased by more than two times from only 0.47 to 1.14 g/cm^3. Correspondingly, an outstanding volumetric capacity of 254 mAh/cm^3 is achieved with the TiO_2/C nanocomposites, which is quite high compared to normal nanostructured TiO_2.

The cyclic and rate performance of the TiO_2 and TiO_2/C composites are presented in Figure 4. As shown in Figure 4a, a significant capacity loss over 50% after 50 cycles regarding the TiO_2 anode prepared with the M_{TTIP} of 0.14, 0.29, and 0.57.

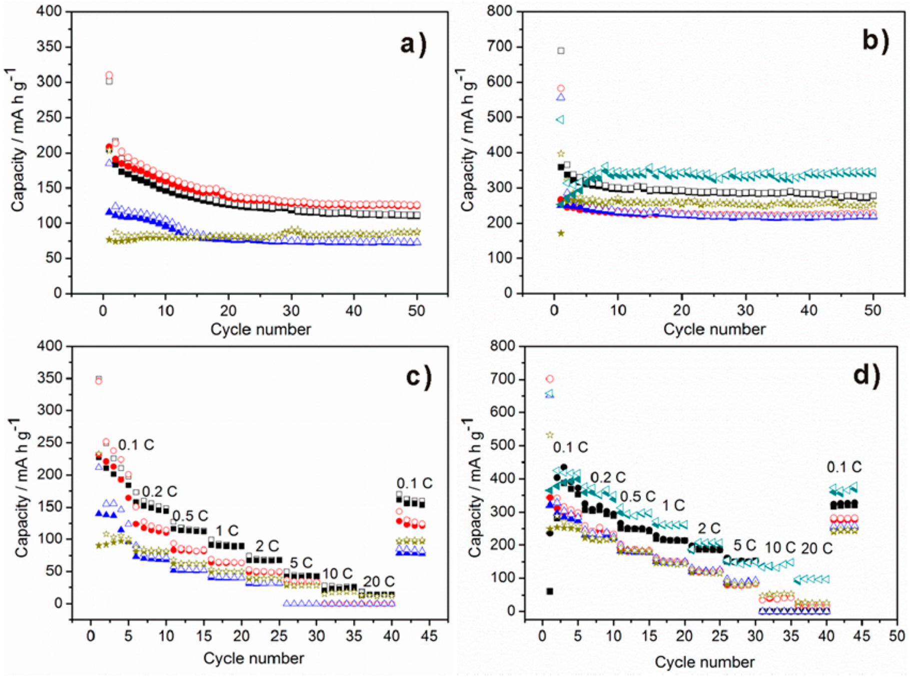

Figure 4. (a, b) Cyclic at 0.2 *C* (1 *C* = 335 mAh/g) and (c, d) rate performance of (a, c) the bare TiO_2 and (b, d) TiO_2/C composites prepared with different M_{TTIP} in the range of 0.005−3 V. M_{TTIP}: black, 0.14; red, 0.29; blue, 0.57, yellow, 1.14; and green, 0. Empty symbol, discharge; solid symbol, charge.

The TiO_2 synthesized with the M_{TTIP} of 1.14 shows a relative stable, but inferior capacity (88 mAh/g). The lack of effective carbon coating on the TiO_2 surface is one of the major reasons for the poor cyclic performance. Besides, The TiO_2 prepared with the M_{TTIP} of 0.14 and 0.29 shows similar cyclic behavior, which are better than that with the M_{TTIP} of 0.57. The results further suggest that the morphology is important for the cyclic performance. Furthermore, the TiO_2 synthesized with the M_{TTIP} of 0.57 exhibits slightly higher capacity than the TiO_2 prepared with the M_{TTIP} of 1.14, but with worse stability. Considering that the morphologies of these two samples are quite similar, the results indicate that the crystallographic phase has a big impact on the capacity of TiO_2. The rutile phase exhibits less capacity but with better cyclic stability compared to anatase.

The TiO_2/C composites show a much better cyclic performance than that of the bare TiO_2 anode (Figure 4b). Capacity loss is observed in the initial cycle mainly due to the formation of solid electrolyte interface (SEI). After 50 cycles, the capacities of the TiO_2/C composites are still in the range between 210 and 280 mAh/g with respect to different M_{TTIP}. The good cyclic stability of TiO_2/C composite may be due to following reasons. First, the TiO_2 nanoparticles with the size of 4−6 nm can effectively accommodate the volumetric change during repeated discharge/charge processes, which is one of the major reasons for capacity fading. Second, the in situ formed carbon matrix provides a good electron conductive matrix and protective layer to the kinetics of the lithiation/delithiation process.

The rate performance of TiO_2 and TiO_2/C composites are shown in c and d in Figure 4. The TiO_2 prepared with the M_{TTIP} of 0.14 and 0.29 show better rate performance at different current densities than the powders prepared with the M_{TTIP} of 0.57 and 1.14, which is due to the worm-like morphology feature. After 5 cycles each from 0.1 to 20 *C*, the capacities can be still recovered to around 170 and 140 mAh/g at 0.1 C. On the contrary, the capacities of only 80 and 100 mAh/g are achieved with the M_{TTIP} of 0.57 and 1.14. The TiO_2/C composites show better capacities at different current densities than TiO_2. It is not only because of the existence of carbon, but also related to the small size and surface carbon coating of TiO_2. Particularly, with the current density up to 5 *C*, the capacities of the TiO_2/C composites with different carbon content can still reach above 100 mAh/g. After 5 cycles each from 0.1 to 20 *C*, the capacities of the TiO_2/C composites can be recovered to the range between 250 and 350 mAh/g at 0.1 *C*. The results indicate that the TiO_2/C composites exhibit good electrochemical cyclic stability.

In conclusion, a new green facile scalable method, inspired by polymeric dental restorative composites, has been developed to synthesize TiO_2/C nanocomposites. TiO_2 nanoparticles with the average sizes of 4−6 nm are homogeneously embedded in the in situ formed carbon matrix with the mass content of TiO_2 varied between 28% and 65%. Conventional dental methacrylate monomers are used as solvent and carbon source, coupled with an energy saving visible light illuminated polymerization process. The electrochemical studies indicate that the discharge/charge behavior of the TiO_2/C nanocomposites has been dramatically modified. Typical plateau of TiO_2 is significantly diminished, where voltage continues to change along with proceeding discharge/charge process. The patterns of the discharge/charge curves resemble the bare carbon. This phenomenon is supposed to be due to the synergistic effect of poor crystallization of TiO_2 and homogeneous embedding of TiO_2 nanoparticles within the carbon matrix. Besides the distinct discharge/charge behavior, the TiO_2/C composite anodes exhibit improved tap density and volumetric capacity compared to bare carbon anode. Good rate and cyclic performance is also achieved with TiO_2/C. Further detailed studies on the optimization of the morphology and LIB anode performance are in progress and will be addressed in future work.

■ ASSOCIATED CONTENT

Supporting Information

Materials, sample preparation, XPS, SEM, EDX, SAXS, cyclic and rate performance of the TiO_2 and TiO_2/C nanocomposites, discharge/charge curves of the TiO_2, and CV curves of the TiO_2 and TiO_2/C. This material is available free of charge via the Internet at http://pubs.acs.org.

■ AUTHOR INFORMATION

Corresponding Author

* E-mail: chengyj@nimte.ac.cn.

Author Contributions

†Y.X. and X.W. contributed equally to this work

Notes

The authors declare no competing financial interest.

■ ACKNOWLEDGMENTS

This research is funded by the Natural Science Foundation of China (51103172), the Zhejiang Nonprofit Technology Applied Research Program (2013C33190), the Program for Ningbo Innovative Research Team (2009B21008), and Ningbo Key Laboratory of Polymer Materials. Y.Y. acknowledges the China Scholarship Council (CSC) and P.M-B acknowledges the funding by the Nanosystems Initiative Munich (NIM) and the Center for NanoScience (CeNS) Munich. Donation of the dental resins from Esstech, Inc., USA, is greatly appreciated.

■ REFERENCES

(1) Chen, Z. H.; Belharouak, I.; Sun, Y. K.; Amine, K. Titanium-Based Anode Materials for Safe Lithium-Ion Batteries. *Adv. Funct. Mater.* **2013**, *23*, 959−969.

(2) Melot, B. C.; Tarascon, J. M. Design and Preparation of Materials for Advanced Electrochemical Storage. *Acc. Chem. Res.* **2013**, *46*, 1226−1238.

(3) Wagemaker, M.; Mulder, F. M. Properties and Promises of Nanosized Insertion Materials for Li-Ion Batteries. *Acc. Chem. Res.* **2013**, *46*, 1206−1215.

(4) Xiao, Y.; Hu, C. W.; Cao, M. H. Compositing Amorphous TiO_2 with N-Doped Carbon as High-Rate Anode Materials for Lithium-Ion Batteries. *Chem.−Asian J.* **2014**, *9*, 351−356.

(5) Menendez, R.; Alvarez, P.; Botas, C.; Nacimiento, F.; Alcantara, R.; Tirado, J. L.; Ortiz, G. F. Self-organized amorphous titania nanotubes with deposited graphene film like a new heterostructured electrode for lithium ion batteries. *J. Power Sources* **2014**, *248*, 886−893.

(6) Yildirim, H.; Greeley, J. P.; Sankaranarayanan, S. Concentration-Dependent Ordering of Lithiated Amorphous TiO_2. *J. Phys. Chem. C* **2013**, *117*, 3834−3845.

(7) Ban, C. M.; Xie, M.; Sun, X.; Travis, J. J.; Wang, G. K.; Sun, H. T.; Dillon, A. C.; Lian, J.; George, S. M. Atomic layer deposition of amorphous TiO_2 on graphene as an anode for Li-ion batteries. *Nanotechnology* **2013**, *24*.

(8) Fang, H. T.; Liu, M.; Wang, D. W.; Sun, T.; Guan, D. S.; Li, F.; Zhou, J. G.; Sham, T. K.; Cheng, H. M. Comparison of the rate capability of nanostructured amorphous and anatase TiO_2 for lithium insertion using anodic TiO2 nanotube arrays. *Nanotechnology* **2009**, *20*.

(9) Hibino, M.; Abe, K.; Mochizuki, M.; Miyayama, M. Amorphous titanium oxide electrode for high-rate discharge and charge. *J. Power Sources* **2004**, *126*, 139−143.

(10) Zhang, Q. F.; Uchaker, E.; Candelaria, S. L.; Cao, G. Z. Nanomaterials for energy conversion and storage. *Chem. Soc. Rev.* **2013**, *42*, 3127−3171.

(11) Chen, X. B.; Li, C.; Gratzel, M.; Kostecki, R.; Mao, S. S. Nanomaterials for renewable energy production and storage. *Chem. Soc. Rev.* **2012**, *41*, 7909−7937.

(12) Zhou, Z. Y.; Tian, N.; Li, J. T.; Broadwell, I.; Sun, S. G. Nanomaterials of high surface energy with exceptional properties in catalysis and energy storage. *Chem. Soc. Rev.* **2011**, *40*, 4167−4185.

(13) Xin, S.; Guo, Y. G.; Wan, L. J. Nanocarbon Networks for Advanced Rechargeable Lithium Batteries. *Acc. Chem. Res.* **2012**, *45*, 1759−1769.

(14) Saito, M.; Nakano, Y.; Takagi, M.; Honda, N.; Tasaka, A.; Inaba, M. Improvement of tap density of TiO_2(B) powder as high potential negative electrode for lithium ion batteries. *J. Power Sources* **2013**, *244*, 50−55.

(15) Chen, D. H.; Caruso, R. A. Recent Progress in the Synthesis of Spherical Titania Nanostructures and Their Applications. *Adv. Funct. Mater.* **2013**, *23*, 1356−1374.

(16) Jiang, J.; Li, Y. Y.; Liu, J. P.; Huang, X. T.; Yuan, C. Z.; Lou, X. W. Recent Advances in Metal Oxide-based Electrode Architecture Design for Electrochemical Energy Storage. *Adv. Mater.* **2012**, *24*, 5166−5180.

(17) Ren, Y.; Liu, Z.; Pourpoint, F.; Armstrong, A. R.; Grey, C. P.; Bruce, P. G. Nanoparticulate TiO_2(B): An Anode for Lithium-Ion Batteries. *Angew. Chem., Int. Ed. Engl.* **2012**, *51*, 2164−2167.

(18) Tan, L. L.; Chai, S. P.; Mohamed, A. R. Synthesis and Applications of Graphene-Based TiO_2 Photocatalysts. *ChemSusChem* **2012**, *5*, 1868−1882.

(19) Froschl, T.; Hormann, U.; Kubiak, P.; Kucerova, G.; Pfanzelt, M.; Weiss, C. K.; Behm, R. J.; Husing, N.; Kaiser, U.; Landfester, K.; Wohlfahrt-Mehrens, M. High surface area crystalline titanium dioxide: potential and limits in electrochemical energy storage and catalysis. *Chem. Soc. Rev.* **2012**, *41*, 5313−5360.

(20) Liu, Y. D.; Goebl, J.; Yin, Y. D. Templated synthesis of nanostructured materials. *Chem. Soc. Rev.* **2013**, *42*, 2610−2653.

(21) Orilall, M. C.; Wiesner, U. Block copolymer based composition and morphology control in nanostructured hybrid materials for energy conversion and storage: solar cells, batteries, and fuel cells. *Chem. Soc. Rev.* **2011**, *40*, 520−535.

(22) Lu, P.; Xia, Y. N. Novel Nanostructures of Rutile Fabricated by Templating against Yarns of Polystyrene Nanofibrils and Their Catalytic Applications. *ACS Appl. Mater. Interfaces* **2013**, *5*, 6391−6399.

(23) Li, W.; Wu, Z. X.; Wang, J. X.; Elzatahry, A. A.; Zhao, D. Y. A Perspective on Mesoporous TiO_2 Materials. *Chem. Mater.* **2014**, *26*, 287−298.

(24) Chen, J. S.; Liang, Y. N.; Li, Y. M.; Yan, Q. Y.; Hu, X. H_2O-EG-Assisted Synthesis of Uniform Urchinlike Rutile TiO2 with Superior Lithium Storage Properties. *ACS Appl. Mater. Interfaces* **2013**, *5*, 9998−10003.

(25) Leprince, J. G.; Palin, W. M.; Hadis, M. A.; Devaux, J.; Leloup, G. Progress in dimethacrylate-based dental composite technology and curing efficiency. *Dent. Mater.* **2013**, *29*, 139−156.

(26) Cheng, Y. J.; Antonucci, J. M.; Hudson, S. D.; Lin, N. J.; Zhang, X. R.; Lin-Gibson, S. Controlled In Situ Nanocavitation in Polymeric Materials. *Adv. Mater.* **2011**, *23*, 409−413.

(27) Yao, Y.; Metwalli, E.; Niedermeier, M. A.; Opel, M.; Lin, C.; Ning, J.; Perlich, J.; Roth, S. V.; Muller-Buschbaum, P. Nano- and Microstructures of Magnetic Field-Guided Maghemite Nanoparticles in Diblock Copolymer Films. *ACS Appl. Mater. Interfaces* **2014**, *6*, 5244−5254.

(28) Ingham, B.; Lim, T. H.; Dotzler, C. J.; Henning, A.; Toney, M. F.; Tilley, R. D. How Nanoparticles Coalesce: An in Situ Study of Au Nanoparticle Aggregation and Grain Growth. *Chem. Mater.* **2011**, *23*, 3312−3317.

(29) Nolan, N. T.; Seery, M. K.; Pillai, S. C. Spectroscopic Investigation of the Anatase-to-Rutile Transformation of Sol-Gel-

Synthesized TiO_2 Photocatalysts. *J. Phys. Chem. C* **2009**, *113*, 16151–16157.

(30) Wang, J.; Zhou, Y. K.; Hu, Y. Y.; O'Hayre, R.; Shao, Z. P. Facile Synthesis of Nanocrystalline TiO_2 Mesoporous Microspheres for Lithium-Ion Batteries. *J. Phys. Chem. C* **2011**, *115*, 2529–2536.